AIAA 2001-0466
Upward Flame Spread Over Thin Solids in Partial Gravity

I.I. Feier*, H.Y. Shih*, K.R. Sacksteder+, and J.S. T'ien*
* Case Western Reserve University, Cleveland OH
+ NASA Glenn Research Center, Cleveland OH

39th Aerospace Sciences Meeting & Exhibit
8-11 January 2001
Reno, Nevada

AIAA-2001-0466

UPWARD FLAME SPREAD OVER THIN SOLIDS IN PARTIAL GRAVITY

Ioan I. Feier*, Hsin-Yi Shih*, Kurt R. Sacksteder+, James S. T'ien*,
* Case Western Reserve University, Cleveland OH 44106
+NASA Glenn Research Center, Cleveland OH 44135

Abstract

The effects of partial-gravity, reduced pressure and sample width on upward flame spread over a thin cellulose fuel were studied experimentally and the results were compared to a numerical flame spread simulation. Fuel samples 1-cm, 2-cm, and 4-cm wide were burned in air at reduced pressures of 0.2 to 0.4 atmospheres in simulated gravity environments of 0.1-G, 0.16-G (Lunar), and 0.38-G (Martian) onboard the NASA KC-135 aircraft and in normal-gravity tests. Observed steady flame propagation speeds and pyrolysis lengths were approximately proportional to the gravity level. Flames spread more quickly and were longer with the wider samples and the variations with gravity and pressure increased with sample width. A numerical simulation of upward flame spread was developed including three-dimensional Navier-Stokes equations, one-step Arrhenius kinetics for the gas phase flame and for the solid surface decomposition, and a fuel-surface radiative loss. The model provides detailed structure of flame temperatures, the flow field interactions with the flame, and the solid fuel mass disappearance. The simulation agrees with experimental flame spread rates and their dependence on gravity level but predicts a wider flammable region than found by experiment. Some unique three-dimensional flame features are demonstrated in the model results.

Introduction

Flame spread is important in understanding both small and large-scale fires. Small-scale fires must be understood and controlled to prevent them from growing into large-scale fires that cannot be tolerated in planetary and spacecraft habitats. Flame spread is divided into two types: opposed, in which the oxidizing gas flows in the opposite direction of the flame spread, and concurrent, in which oxidizing gas flows in the same direction as the flame spread. Both concurrent and opposed gas flows may have forced and buoyant flow components. For buoyant cases, concurrent flame spread is equivalent to upward flame spread and opposed is equivalent to downward.

Recent interest on microgravity combustion has resulted in a number of experimental studies of flame spread in low-speed forced flow. However, with the exception of Sacksteder and T'ien[1] who investigated downward spread in partial gravity, there is little work on flame spread in a purely buoyant partial gravity environment. Besides the contribution to combustion science, the understanding of flame spread in partial gravity can be important to fire safety in future missions to mars or the moon, or in spacecraft with artificial gravity.

To obtain accurate qualitative and quantitative solutions to flame spread, both concurrent and opposed flow flames require numerical models incorporating rigorous treatment of the fluid dynamics, fuel pyrolysis mechanisms, gas phase finite rate kinetics and radiation. Numerical results must be compared to experimental data to validate the theories and approximations made in the model.

There have been only two variable buoyancy flame spread experiments. Partial gravity flame spread data is limited to the opposed work of Sacksteder and T'ien[1]. They investigated buoyant downward flame spreading in 0.05-1.0 g/g_e using 5-cm wide Kimwipes tissue paper samples with the same experimental apparatus used here. (For brevity, 1.0 G is defined throughout the paper as 1.0 g/g_e where g_e is the acceleration due to normal earth gravity.) Sacksteder and T'ien compared their data to Altenkirch et al.[2], who studied downward flame spread over index cards and adding-machine tape in elevated gravity centrifuge environments from 1 to 4 G.

Other experimental investigations exist for buoyant, normal gravity upward flame spread over thin solid fuels. Large-scale flame spreading over wide cotton samples was initially laminar but then transitioned to turbulent behavior without reaching steady state[3]. Upward flame spreading on narrow paper samples, up to 2-cm width, can reach steady state in reduced pressures in normal gravity[4]. The mechanisms of steady vs. unsteady spread remains a contemporary

research topic[5]. There are also many downward flame spread experiments in normal gravity that will not be discussed here.

Most numerical models compared with experiments have been two-dimensional (2-D) and forced flow. Ferkul[6,7], used Navier-Stokes elliptic treatment in the flame stabilization region matched to parabolic equations in the downstream region to model two-dimensional (2-D), concurrent, laminar, forced flow, flame spread over a thin solid. Jiang[8] improved on Ferkul's model with full elliptic Navier-Stokes equations and added a flame radiation model.

In addition to forced flow, limited computation for two-dimensional upward buoyant spread has been made in reduced gravity (between microgravity and 0.10 G)[9]. Steady, constant length flames have been found although these 2-D, normal-pressure flames become very long as gravity approaches 0.1 G. The computed results suggest that the spread rate and the flame length are approximately proportional to the gravity level. Numerical models also exist for opposed flame spread, but they are not discussed here.

This paper investigates upward, steady flame spread over a thin solid fuel in partial gravity environments with steadily propagating flames. The effects of gravity, sample width, and pressure on flame spread and structure are analyzed. Partial gravity levels investigated are 0.10 G, Lunar G (0.16 G), Martian G (0.38 G), and normal 1-G. Qualitative flame behavior and structure are discussed. Quantitative data such as spread rates are presented.

The experimental results are compared to results from a three-dimensional (3-D) numerical model thought to represent the important physical phenomena in the experiment better than previous 2-D attempts. The model used here has been recently developed by Shih[10,11] to examine steady laminar flame spread and extinction over a thin solid fuel in low-speed forced concurrent flows. Extension to a purely buoyant case in partial gravity at reduced pressures has been carried out in this paper to provide comparisons with the experimental results and to provide additional insight on the three-dimensional features of upward flame spreading. This model will be discussed in more detail later in the paper.

Experiments

Observations of flame spread over a thin cellulose fuel were made in reduced-pressure air environments in normal gravity and in partial-gravity simulations using the GIFFTS test apparatus[1] with slight modifications.

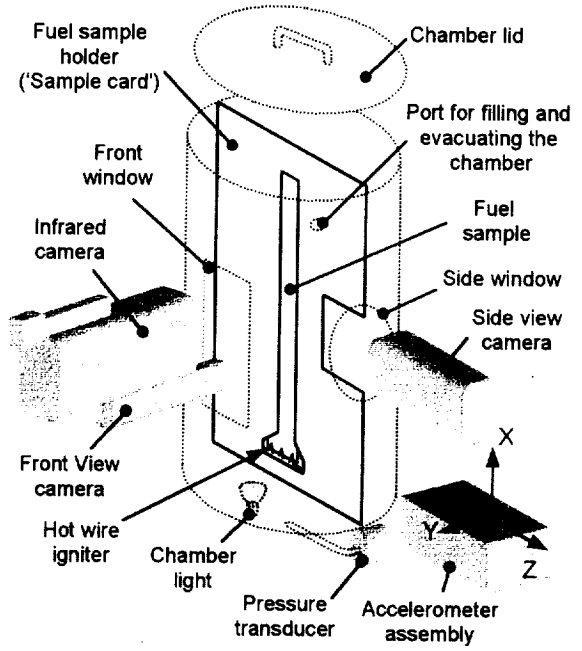

Figure 1: Experimental setup - including the combustion chamber and surrounding hardware. Chamber is 25 cm in diameter and 53 cm high.

Figure 1 shows a system schematic including the 27-liter cylindrical combustion chamber (25.4 cm diameter, 53.2 cm height), video cameras for imaging the fuel surface and edge, the infra-red camera for imaging the fuel surface and the three-axis accelerometer module. An embedded computer controlled the experiment sequence: chamber air evacuation and filling, video time-code initiation, igniter activation, and the recording of digitized pressure and acceleration data. Chamber pressure, igniter duration times, and test duration times were preset by the operator for each test.

Fuel samples were a thin cellulosic tissue with the trade name of "Kimwipes EX-L, Delicate Task Wipers" manufactured by the Kimberly-Clark Corporation, product number 34256. The fuel samples were cut into rectangular pieces and mounted with clear adhesive tape over the opening in the stainless steel sample holders. Sample holders were fashioned to expose 1-cm, 2-cm or 4-cm widths (on both faces of the sample) of the fuel to the chamber atmosphere. The dominant tissue fiber direction, determined by inspection under a microscope and the preferential tear direction, was oriented perpendicular to the flame spread direction. Preliminary tests in normal gravity showed that orienting the fuel this way reduced cracking of the fuel during burning and the irregular shape of the fuel burnout edge.

In earlier work[1] fuel samples were dried by exposure to chamber vacuum before and during aircraft takeoff, then stored until use in the cabin atmosphere at the testing altitude - where the relative humidity is low. In this work, an improved sample drying procedure consisted of using a hot-air gun to insure rapid, thorough, and more consistent drying. The fuel sample holder was shielded from the hot air flow to minimize heat transfer to the metal sample card.

Samples were installed in the test chamber, which was then sealed and filled with air at pressures between 0.2-0.4 atmospheres. The test atmospheres were established using primary standard, precision mixtures of 21% O_2, balance N_2, certified to +/- 0.02% O_2 by the vendor. The combustion chamber was filled to the desired test pressure under computer control that maintained the desired pressure during the temperature equilibration of the incoming gas.

The samples were ignited using resistive heating of 0.27-mm diameter (29-gauge) Kanthal wire, 12 cm long, shaped in a zigzag pattern and interleaved with the bottom edge of the fuel samples. The 2.5 Ω igniters were energized with 28 VDC for 1/3 sec.

Flight tests were performed onboard the NASA KC-135 Reduced Gravity Aircraft[12]. Parabolic flight trajectories provided a simulated reduced-gravity environment between 20-45 sec. depending on pilot skill and weather. Up to ten partial gravity parabolas were obtained per flight at nominal accelerations levels of 0.1, 0.16, and 0.38 G.

The chamber pressure and three axes of accelerations were recorded by the GIFFTS computer at 30Hz. Pressure measurement resolution of 0.001 atm and the chamber filling algorithm ensured repeatable test pressures. Acceleration measurements were recorded to resolutions of approximately $6x10^{-5}$G.

The front and side video cameras provided color imaging recorded on conventional S-VHS videotape. A Prism DS infrared (FSI Inc.) camera with a flame filter was used to record 12-bit digital video of the solid surface at 30 frames per second. The bandpass flame filter centered at 3.8μm was used to reduce the detection of gas-phase emissions (e.g. from H_2O, CO_2). The CaF window facing the IR camera was chosen to pass radiation in the 3-5μm band in addition to visible wavelengths. The fields of view of the cameras were similar; however due to physical constraints the side view camera was mounted closer to the top of the chamber. During a test the flame would first appear in the front field of view, and only later in the side and IR fields of view.

The video imaging data was analyzed using the Tracker 3.0 software/hardware system developed at the NASA Glenn Research Center[13]. This package tracks the displacement of selected flame elements from video frame to frame and records their position for later determination of flame velocity and size. The package can be configured to automatically track a flame element based, for example, on its brightness. However, the tips of most flames observed in these tests were too dim to use this method and their positions were determined by manual inspection of the video images.

Experimental Results

Acceleration Environment

Figure 2 shows the measured vertical accelerations beginning in each case with the manual initiation of the experiment. The dashed lines indicate the target acceleration levels of 0.10, 0.16, and 0.38 G. Times of 5-20 seconds were observed during which acceleration levels remained within 15% of the nominal value. Tests with larger g-jitter were discarded. The duration of the partial-gravity aircraft maneuver generally increases with the intended acceleration level[1].

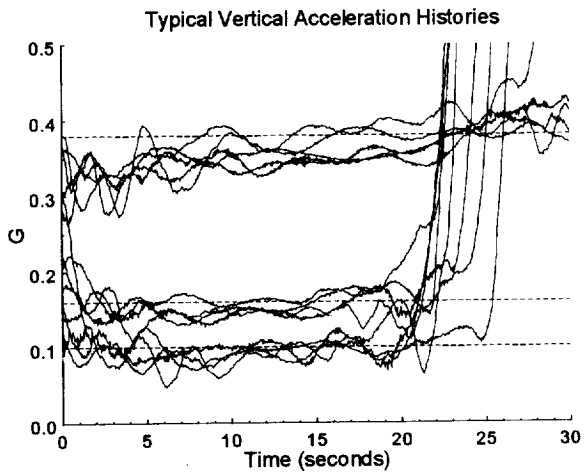

Figure 2: Typical vertical acceleration histories for 0.10 G, 0.16 G (Lunar) and 0.38 G (Martian) tests.

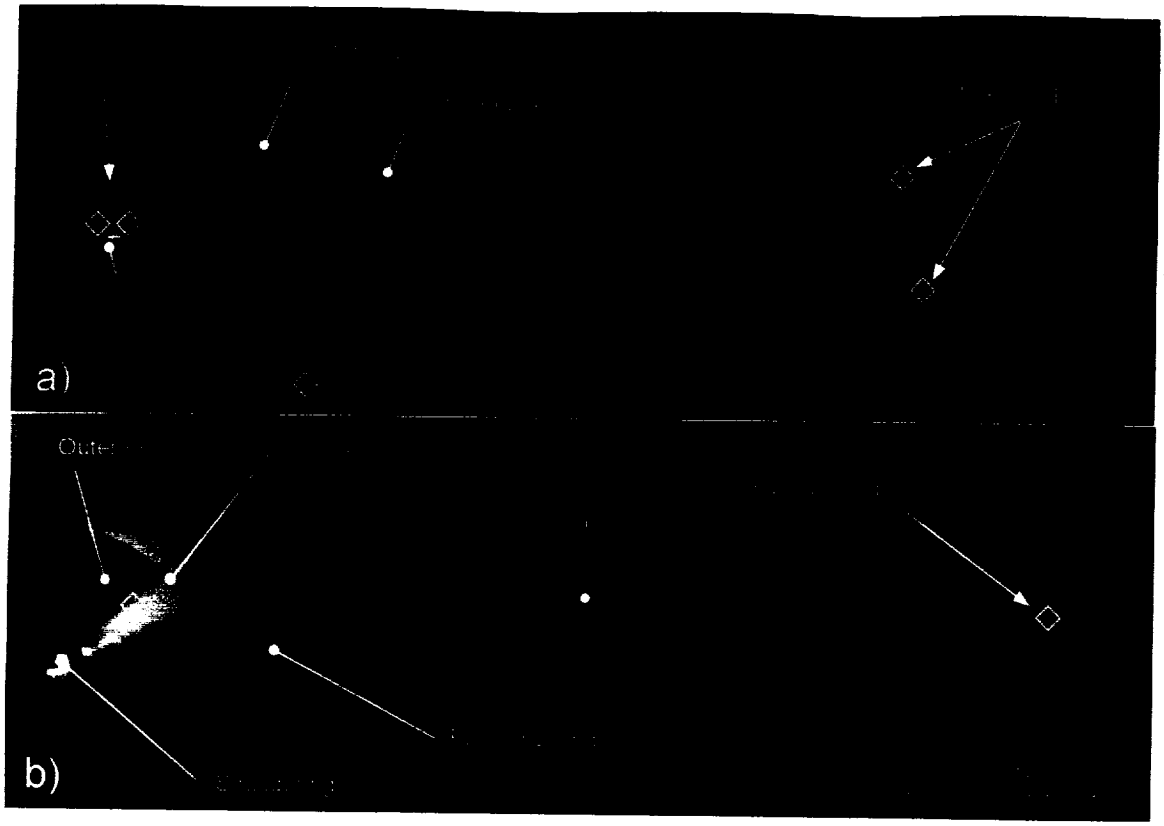

Figure 3: Flame spread is towards the right. Gravity is towards the left. Representative flame tracking points are shown by the diamonds. Scale is approximate. **a) (Top)** Side (edge) view of Martian gravity (0.38 G) 2-cm flame spread at 0.27 atm (4.0 psia). **b) (Bottom)** Front view of Martian gravity (0.38 G) 2-cm flame spread at 0.27 atm (4.0 psia)

Flame Structure

Figure 3 shows the side and front views of a flame spreading upward over a 2-cm wide sample in 0.38 G and 0.27 atm (4.0 psia) air; the upward spread is shown here from left to right. Figure 3a shows the side view (i.e. the fuel edge); figure 3b shows the front view (the fuel surface). In the side view an inner and an outer flame are visible. The inner flame is blue; the outer flame is upstream (to the left) and is a light orange or yellow. Because the base (bottom) of the flame is not straight or in line with the side-camera viewing angle, the flame appears thicker. Much of the flame length is approximately parallel to the fuel surface. The flame tips are indicated with the red diamonds. For short flames, flame shapes were steady and regular. Longer flames exhibited oscillating tips and irregular shapes.

The tip of the pyrolysis zone is indicated with the yellow diamond in the front view as the downstream beginning of visibly blackening fuel. The pyrolysis fronts and flames were peaked near the fuel centerline. In the region indicated as the burnout zone, fuel cracking and local burnout was evident to some degree in all tests; the severity increased for wider samples. In some instances, the pyrolyzing fuel curled near the burnout. Close to the edge of the metal sample holder, fuel pyrolysis was quenched but the fuel smoldered after the flame passed. In the upper left of the side view, some fuel has curled upward in the base region and is responsible for the orange color there. In cases where the burnout front was not uniform, a representative location was chosen to be halfway between the most and least advanced burnout locations.

Figure 4 shows the effects of pressure and gravity on side-view flame appearance. As gravity increased the visible flame length and intensity increased. Flame length also increased with pressure. The downstream portions of the longer flames were almost parallel to the solid fuel, i.e., a constant flame standoff distance. The self-similar boundary layer solution presented by Jiang et al. suggested increasing downstream flame standoffs from the fuel surface[14]. The somewhat

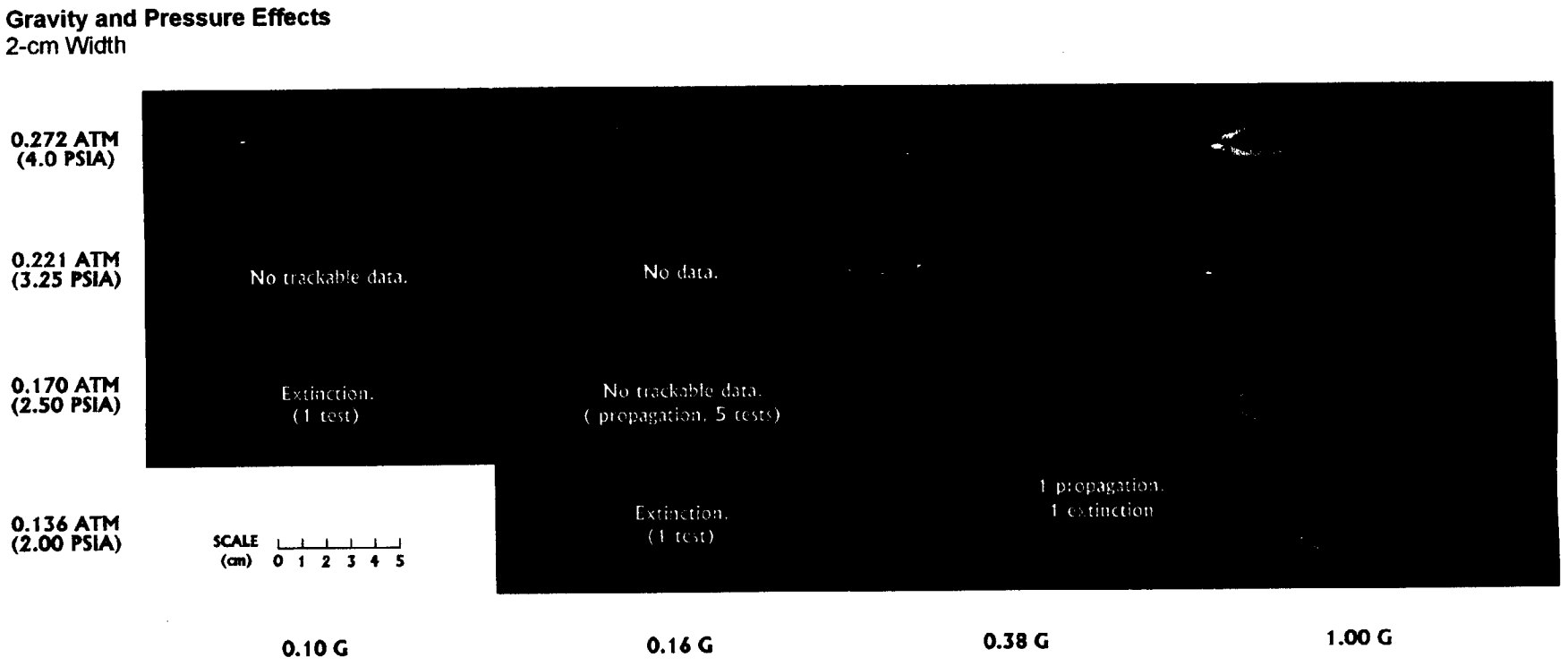

Figure 4: Side images of 2-cm width flame propagation at various pressures and G levels. Flame propagation is towards the right.

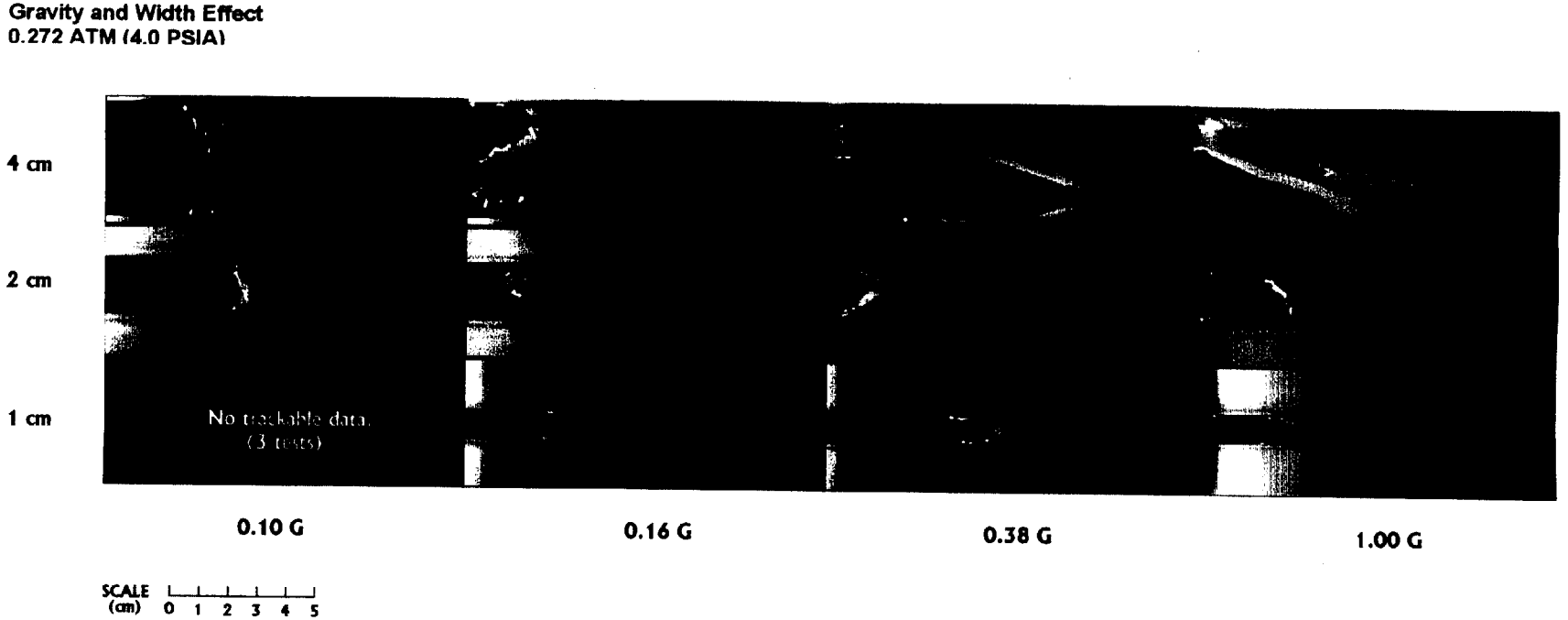

Figure 5: Front images of flame propagation at 0.272 ATM (4.0 PSIA). Flame propagation is towards the right.

irregular flame bases at higher pressures in 1 G are the consequence of uneven burnout. Some of the bright spots on the left side of the flames are due to smoldering and fuel curling.

Figure 5 shows the effects of sample width and gravity. The front view does not show flame lengths well, but the pyrolysis zone lengths and shapes are clear. Increasing width or gravity increased the pyrolysis length. The flames, pyrolysis fronts and burnout fronts of the narrower samples burned symmetrically about the fuel centerline even if the ignition was not uniform. With increasing width, the samples burn less uniformly, especially the burnout front, which tends to advance more quickly along one side of the sample or the other.

Flammability Limits

Reducing the gravity level or pressure caused extinction. At a given gravity level, the extinction pressure depends on sample width. A flammability chart for 2-cm wide samples burning upward in reduced pressure and partial gravity is shown in Figure 6, where time-averaged test pressures are plotted vs. time-averaged vertical gravity levels. For tests that ended with extinction the 5 seconds before extinction was used to compute the pressure and gravity averages. Successful propagation was defined as flame spread over more than 3/4 of the sample length. Successful tests are indicated with triangles; those ending with extinction are indicated with crosses.

In cases of incomplete propagation, the distance that flames spread before extinction was determined to be a function of the initial test pressure. In normal gravity at pressures above 0.15 atm, the entire sample burned while for pressures below approximately 0.10 atm, the fuel extinguished immediately after the promoted ignition. The shaded area in figure 6 indicates this transition from full to null propagation, which is attributed to oxygen depletion in the finite chamber. In between these pressures, the fuel was partial consumed. A similar transition seems apparent in partial-gravity environments, but this observation is based on a limited number of tests.

Figure 7 shows a comparison of the experimentally determined flammability boundaries for 1-cm, 2-cm and 4-cm width samples. The wider samples were more flammable, i.e., for a given gravity level the fuel burned at lower pressures. Above 0.38G the flammability is affected less by gravity. For lower gravity levels, the flammability limits occurred at higher pressures, especially for 1 and 2-cm samples.

Spread Rates

The flame spread rates were computed from the flame-position vs. time data obtained using the Tracker software. The spread rates reported here are for the mid-point between the flame base and tip. The difference between the flame tip and base locations yields flame length for the side view and the length of the blackened region yields the pyrolysis length for the front view. In the side views the tip position is obtained by averaging the upper and lower flame tip locations, and base location is obtained by averaging the leading and trailing bases; all shown in Fig. 3a.

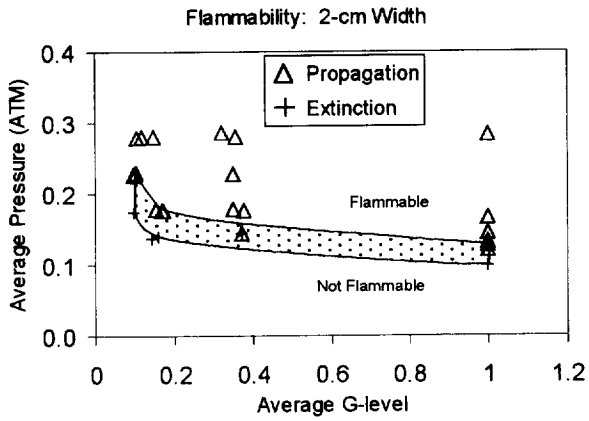

Figure 6: 2-cm width flammability limit.

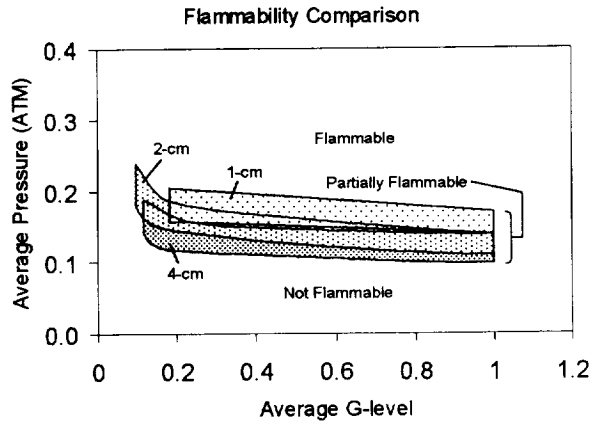

Figure 7: 1-cm, 2-cm, and 4-cm, flammability comparison.

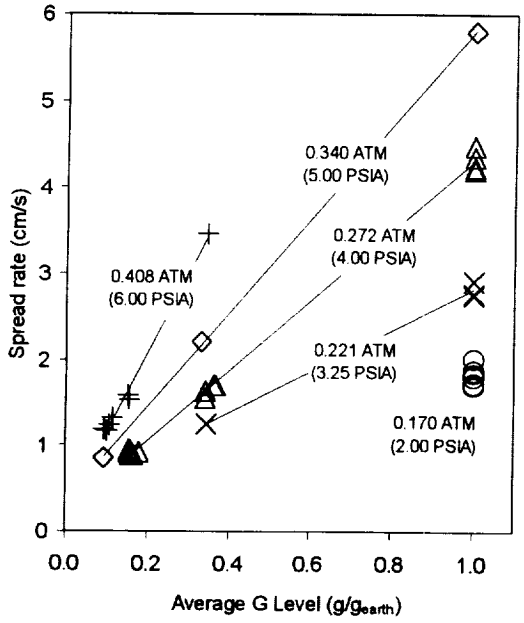

Figure 8: [1-cm width] spread rates vs. G for various pressures.

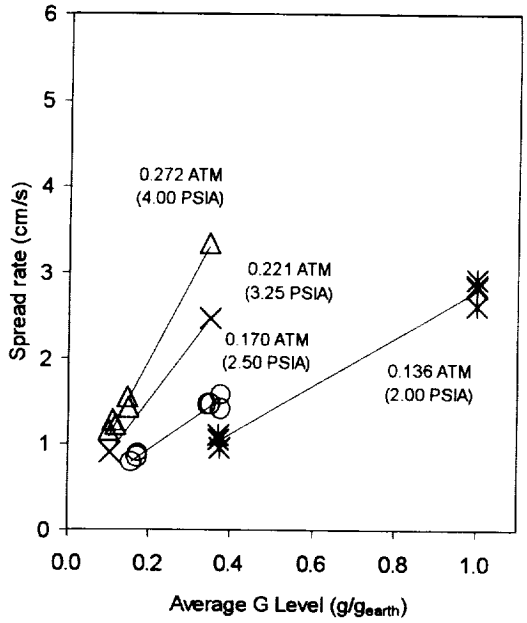

Figure 9: [2-cm width] spread rates vs. G for various pressures.

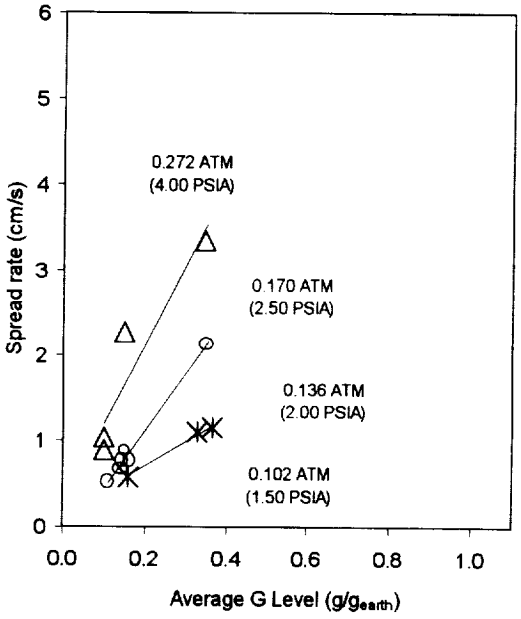

Figure 10: [4-cm width] spread rates vs. G for various pressures.

The spreading rates reported here are for those tests that yielded steady spreading rates including the propagation speed of the flame tips and base and/or the pyrolysis front. The plots in Figures 8-10 are composite plots including the spread rates of the flame midpoints and/or the pyrolysis midpoint without specifically distinguishing between these data types. Consistent flame and pyrolysis spread rates were found for tests where both front and side tracking could be performed. For some tests, only the pyrolysis could be tracked because the slowly propagating flames did not reach the side view before the end of the parabola. The average gravity level is shown and was calculated by time-averaging the local vertical acceleration during the same time that the flame position was recorded. Some spreading flames that could be analyzed for position data were not included in the spread rate results because they were determined to have unsteady spread rates (most were 4-cm cases). A further discussion of steadiness may be found in the corresponding thesis[15].

Flame spread rates for the 1-cm wide samples are shown in Figure 8 plotted versus gravity level for various pressures. Increasing the gravity level increased the spread rates linearly; the effect of gravity is stronger at higher pressures. Figure 9 shows spread rates for the 2-cm width samples, and figure 10 for 4-cm width samples. While the same trends in spread rate with gravity and pressure are indicated for these

wider samples, the flame lengths were too large to yield reliable spread rates above the gravity levels shown.

Numerical Model Description

A three-dimensional model was recently developed to simulate steady laminar flame spread and extinction over a thin solid fuel in low-speed forced concurrent flows[10]. That model has been extended to simulate the purely-buoyant flow case in partial-gravity, reduced-pressure environments for comparison with the evolving experimental results and to provide additional insight into the details of three-dimensional upward spreading flames.

The numerical model of the gas phase solves the full three-dimensional, steady, and laminar Navier-Stokes equations for the conservation of mass, momentum, energy and species. The species equations include fuel vapor, oxygen, carbon dioxide and water vapor. The gas-phase reaction is represented by one-step, second-order finite rate Arrhenius kinetics. The activation energy and pre-exponential factor are 1.13×10^5 J/g mol and 1.58×10^{12} $cm^3/g/s$ respectively; the heat of combustion is 1.675×10^4 J/g.

The thermally-thin solid model consists of continuity and energy equations whose solutions provide the boundary conditions for the gas phase. The solid pyrolysis is approximated by a one-step, zeroth-order decomposition obeying an Arrhenius law, where the activation energy and pre-exponential factor are 1.256×10^5 J/g mol and 3.8×10^7 cm/s respectively. The consumption of the solid phase is modeled by a reduction in fuel thickness. Gas-phase radiation is neglected, but the solid radiative loss with an emissivity of 0.92 is included in the model. The detailed description of the mathematical model including the governing equations, and the thermal and transport properties can be found in Shih[10].

For this paper, upward flame spread over a 2-cm wide solid fuel was simulated with a 4-cm inert sample holder on each side of the fuel sample in the same vertical plane. The fuel sample and holder were located in the middle of a square cross section (10x10 cm), open-ended duct (34 cm long) – a configuration derived from the preceding forced-flow model cqnfiguration. The gravity vector pointed in the negative X-direction (downward). The temperature of the sample holder and the tunnel walls were fixed at 300K, a good approximation since both the sample holder and the wall have much larger thermal inertia than the fuel. Symmetry was assumed in both central and vertical planes, one occupied by the fuel, the other by its perpendicular bisector. This convenient symmetry reduced the solution domain to one quarter of the duct volume. The simulation used a flame-fixed coordinate system achieved by feeding the fuel into the flame at the necessary rate for a steady flame solution[16]. The flame base position was fixed at 10 cm above the tunnel entrance. The typical three-dimensional computational grid contained about 180,000 points ($75 \times 40 \times 60$). Approximately 160 hours of CPU time on the Compaq XP1000, 667 MHz workstation was needed for convergence of each steady flame configuration.

Comparison of Numerical and Experimental Results

The numerical simulations of upward flame spread were completed for 2-cm wide solid samples with the approximate properties of the Kimwipes materials used in the experiments. The flame-spreading environment was 21% oxygen, balance nitrogen (air) at 0.272 atm (4.0 psia) pressure for three distinct gravity levels (0.1, 0.16, 0.38 G). A detailed comparison of the experimental and numerical results of the 0.16 G case is shown. Trends in flame spread rate, flame and pyrolysis lengths, and extinction limits with variations in gravity level are shown and compared to the experimental results.

Numerical simulations with one-step global reactions have predicted the visible appearance of experimental flames best through calculated reaction rate contours. Since this model is three-dimensional, integrating the calculated reaction rate across the width of the flame provided a two-dimensional reactivity contour representation most equivalent to the experimental side view image, better than contours at an arbitrary plane cut through the flame. Figure 11 shows the side view image of a flame spreading upward in air at 0.272 atm and 0.16 G and the integrated fuel reactivity contours. The simulated and experimental flame shapes seem to agree except for the downstream flame standoff distance from the fuel where the computed distance is slightly larger than experimentally observed.

Figure 12 shows the front image of the experimental flame and the solid thickness profile predicted by the simulation. The blackened solid pyrolysis region and burnout shapes are visible. The contours represent the unburned fuel fractions increasing from left to right from 0% to 99%. The 0% curve indicates the burnout front where the fuel is completely consumed. There is good qualitative agreement of the two-dimensional pyrolysis pattern and the burnout shape between the experiment and the simulation.

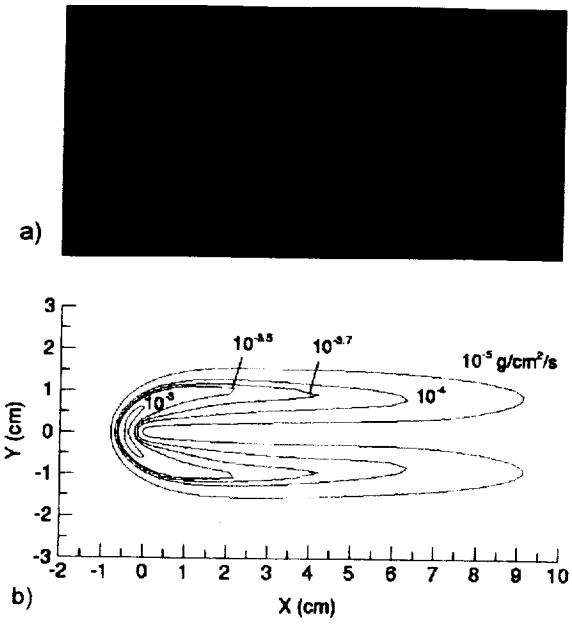

Figure 11: [2-cm, 0.16 G, 0.27 atm case]
a) Experimental flame side view image.
b) Computed fuel reactivity contours (integrated over flame width).

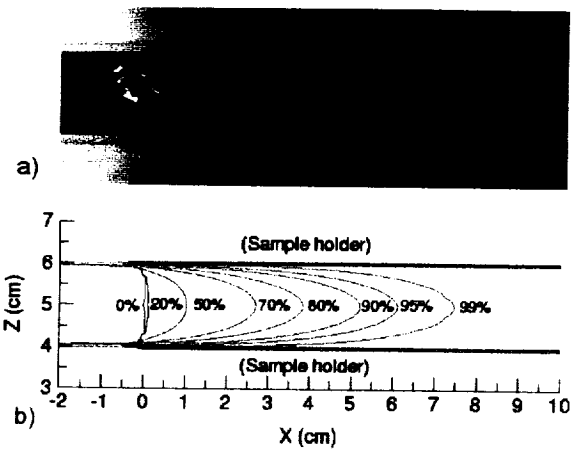

Figure 12: [2-cm, 0.16 G, 0.27 atm]
a) Experimental front view image.
b) Computed solid thickness profile from model.

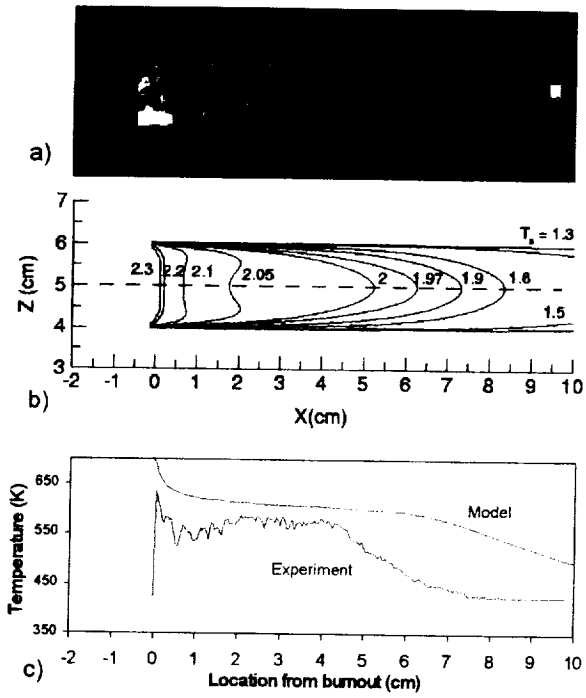

Figure 13: [2-cm, 0.16 G, 0.27 atm]
a) Equivalent blackbody temperature profile from experiment. The camera sensitivity limits the lowest detectable temperature to 423K.
b) Fuel surface temperature contours from numerical model.
c) Comparison of centerline temperature profiles for above.

Fig. 13(a) shows the infrared (IR) image of the solid shown as the equivalent blackbody temperature measured through a narrow band pass filter at 3.8μm wavelength and normalized by 300K. The computed solid temperature contours, also normalized by 300 K, are shown in Figure 13(b). The temperature profiles along the fuel centerline are given in Fig. 13(c).

The computed and experimental two-dimensional temperature profiles in Figures 13(a) and (b) are qualitatively similar; but there are quantitative differences shown in (c). The computed surface temperatures in the pyrolysis zone are higher than the equivalent blackbody temperature indicated by the camera detector. Surface emissivity less than unity would increase the temperatures indicated by the camera data, but the actual emissivity of partially pyrolyzed Kimwipes material at elevated temperatures is not known.

The large slopes in the downstream regions of both temperature profiles indicate where the fuel is preheated to the pyrolysis temperature. The end of the preheat zone is indicated by the transition to a comparatively flat temperature profile. The transition point can be called the pyrolysis front and its distance from the fuel burnout called the pyrolysis length. In Fig. 13(c) the computed pyrolysis length (~6.2 cm) is considerably longer than the experimental length (~4.5 cm). A previous 2-D flame-spread simulation[8], showed that including flame radiation in the model shortens the flame and pyrolysis lengths in low-speed flow with little affect on the spread rates. Additionally, there are uncertainties in the kinetic-rate constants for both the solid pyrolysis and the gas reactions.

Solving the Navier-Stokes equations allows detailed study of the flame structure. Figure 14 shows the flow field around the flame in the plane perpendicular to the fuel centerline (Z = 5 cm). Because of the symmetry with respect to the solid, the upper half of the figure shows velocity vectors and temperature isotherms and the lower half shows velocity streamlines, oxygen mass flux vectors and the fuel reaction rate contours.

Downstream the temperature contours are nearly parallel to the solid, starkly different from the purely forced-flow case in microgravity where the downstream flames diverge from the fuel. In a buoyant environment, flow is driven by density gradients and accelerates strongly inside the flame zone. The flow velocities shown in Figure 14 are about 10 cm/s near the entrance but accelerate to 60 cm/s in the flame zone. Upstream, the streamlines first deflect away from the solid because of the pressure increase created by the stagnation point and fuel vapor blowing from the surface in the flame stabilization zone. The streamlines then bend toward the solid due to flow acceleration in the flame zone. Qualitatively, this is quite different from that in the purely forced flow where the streamline is always directed away from the solid unless the flow is confined by an excessively small wind tunnel[8,10,17].

Upstream, the oxygen mass flux is dominated by the convective transport; and the oxygen mass flux vectors and the velocity streamline point in the same direction. Near the flame zone, however, the oxygen mass flux vector deviates from the streamline, indicating a strong diffusion of oxygen into the flame.

The flame structure in the centerline plane perpendicular to the fuel is qualitatively similar to the two-dimensional model[9]. Some unique three-dimensional features of the flame are revealed by also examining the flow field around the flame in a vertical plane parallel to and 1 cm away from the solid, as shown in Figure 15. Because of symmetry the top half of the figure shows the velocity streamlines, oxygen mass flux vectors and the fuel reaction rate contours; the bottom half shows the flame temperature and the projections of the velocity vectors on this plane. Because the flow field is purely buoyant, the gas accelerates throughout the length of the flame, entraining air from the sides and pulling the streamlines toward the central plane. Flow re-circulation exists on the side of the flame that would not appear in a two-dimensional simulation. There is significant diffusion of oxygen from the side to the flame, comparable in magnitude with the convective oxygen stream. This lateral diffusion is impossible in the two-dimensional simulation[10,11].

A comparison of computed and experimental flame spread rates as a function of gravity level is shown in Figure 16. Both model and experiments indicate that flame spread rate increases linearly with gravity level. The comparison between experiments and model can be considered excellent both quantitatively and qualitatively.

The flame and pyrolysis lengths can also be compared at these three gravity levels. In the three simulations presented here, an unburned fuel fraction of 95% consistently occurs at the transition from the pyrolysis to preheat regions based on the slope of fuel surface temperatures, which was chosen as the computed pyrolysis front. The integrated fuel reactivity contour of 10^{-4} g/cm^2/s (that was shown in Fig. 11) was chosen to represent the boundary of the visible flame. In the experiment, the visibly blackened solid represents the pyrolysis region. The pyrolysis lengths

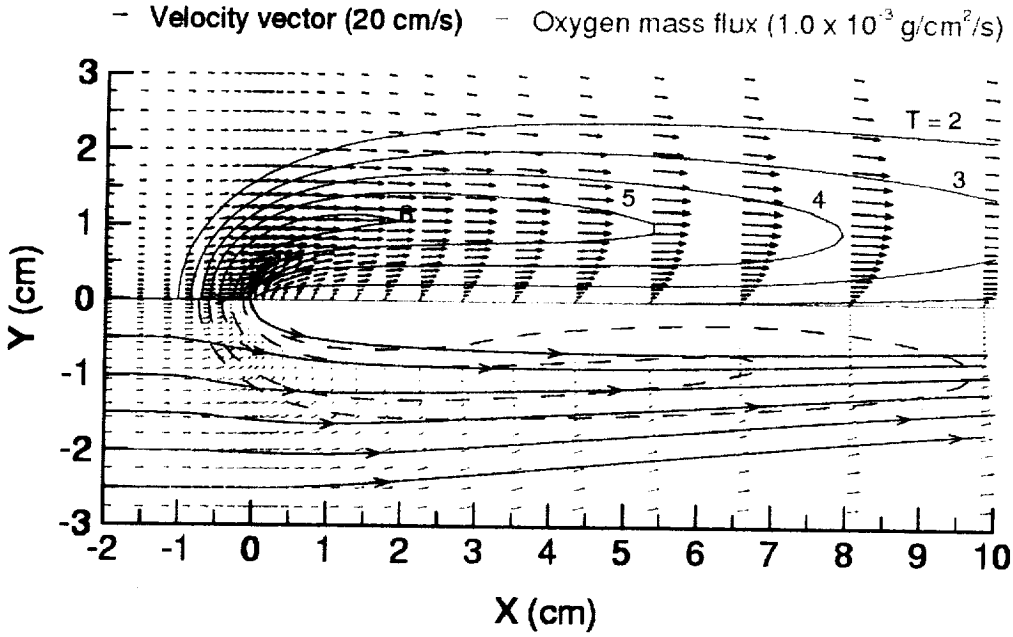

Figure 14: [2-cm, 0.16 G, 0.27 atm] Two-dimensional slice perpendicular to fuel surface. Top half: flow field, nondimensional temperature (1 unit = 300K). Bottom half: streamlines, oxygen mass flux, and fuel reaction rate contours (10^{-5}, 10^{-4}, 10^{-3} g/cm^3/s from outermost).

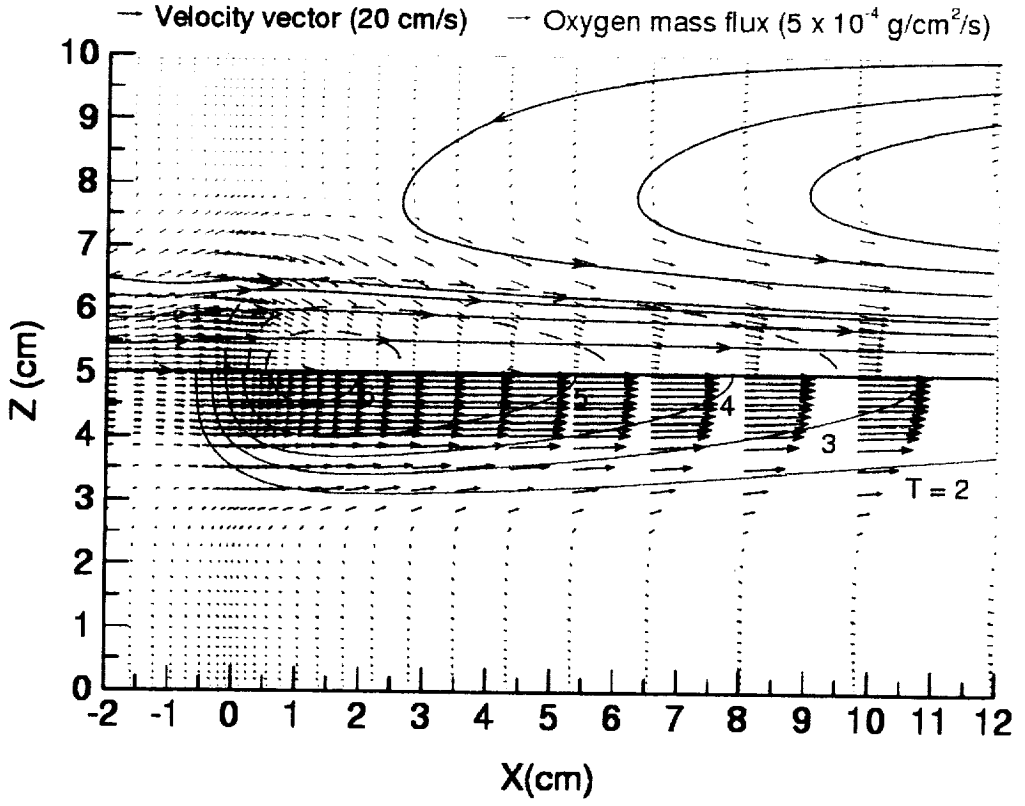

Figure 15: [2-cm, 0.16 G, 0.27 atm] Two-dimensional slice in a plane parallel to solid fuel, 1-cm above. Top half: velocity streamlines, oxygen mass flux vectors, fuel reaction rate contours (10^{-5}, 10^{-4}, $10^{-3.5}$ g/cm^3/s from outermost). Bottom half: nondimensional flame temperature (1 unit = 300K), velocity vector projections on plane.

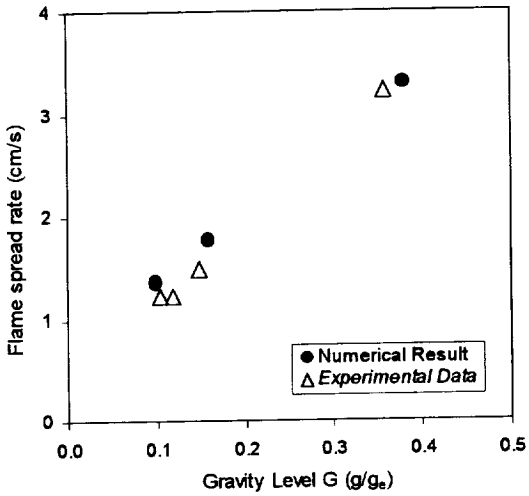

Figure 16: Martian, Lunar and 0.10G comparison of spread rates for numerical and experimental cases for 2-cm, 0.27 atm.

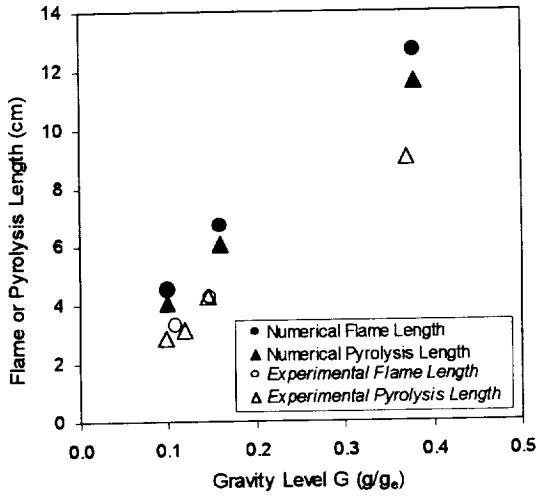

Figure 17: Martian, Lunar, and 0.10G comparison of pyrolysis and flame lengths. Numerical flame lengths are based on integrated reaction rate contours of 10^{-4} g/cm^2/sec. Pyrolysis lengths are based on an unburned fuel fraction of 95%.

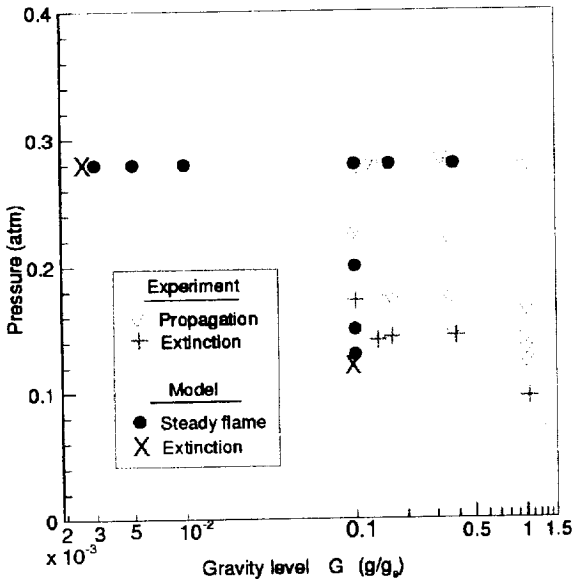

Figure 18: Comparison of experimental flammability limit and numerical limits. An extinction pressure limit was determined for 0.1 G, and an extinction gravity limit was determined for 0.272 atm (4.0 psia) using the numerical model.

from visible images agree within 10% of the lengths determined by the slope transition of the equivalent blackbody temperature in the IR camera image. Experimental flame lengths are measured from the visible video images.

Figure 17 shows a comparison of computed and experimental pyrolysis and flame lengths. The computed lengths are slightly longer than the experimental lengths. Both the simulation and experiments show that the pyrolysis and flame lengths increase linearly with gravity level.

The flame-spread simulation was also used to estimate flammability boundaries that are reached by reducing pressure or the local gravity level. In the simulation, the boundary is determined by failure of the computation to converge to a steady solution. The experimental flammability data in Fig. 6 is re-plotted in Figure 19 together with the computed solutions. At a gravity level of 0.10 G, the model predicted extinction at 0.12 atm pressure, lower than the experiments indicated. A low gravity extinction limit was determined at a pressure of 0.272 atm, where the flame went out at 2.5×10^{-3} G. Due to g-jitter, this gravity level is below what can be accessed using the aircraft.

Discussion

A combined experimental and theoretical modeling approach has been employed to investigate the upward flame spread phenomena over a solid in partial gravity including Lunar and Martian gravity levels. The partial gravity experiments were conducted in an airplane flying parabolic trajectories. Since the partial gravity duration is limited, the solid fuel chosen is Kimwipes tissue- a very thin solid. Because of g-jitter, there is also a low-g limit for the experiment (approximately 0.1 earth gravity). Using a three-axis accelerometer, the g-jitter has been carefully monitored and the results presented are within an acceptable g-variation.

In the experiments, upward spreading was studied with sample width, total pressure and gravity level as parameters. Limited by the combustion chamber size, small-scale, constant-flame-length, steady spreading conditions were found when the samples were relatively narrow, the pressure was low, and/or g-level was reduced. These are the flames studied in detail here.

A low-pressure extinction limit exists for a given gravity level and sample width. There is also an indication of low-g extinction limits at sufficiently low pressures. An approximate flammability boundary is presented. However, the experimentally determined boundary is incomplete because of limitations on the low-g level that can be achieved in the airplane without substantial g-jitter.

A detailed three-dimensional upward flame spread model in laminar flow has been formulated and numerically solved. It has been used to compare with the experimental data and to provide additional insight on the spreading flame structures. The model consists full Navier-Stokes, equations, a finite-rate one-step gas-phase reaction, a solid pyrolysis decomposition reaction and surface radiation loss. The model solution yields details of the three-dimensional gas-phase flow field, oxygen transport, temperature and species distributions in addition to two-dimensional surface temperature and thickness profiles and burning rate distribution. Comparisons with experiments have been made wherever the experimental data are available.

Both experiment and model suggest that the flame spread rate, the flame and pyrolysis lengths are proportional to gravity level (within the range tested). The proportionality constants may vary with pressure and sample width. Quantitative agreement between experiment and model exists for flame spread rates. Spread rate appears to be the least sensitive parameter to the details in the model.

Comparing with the experimental infrared surface image, the pyrolysis front picture and the flame photograph suggest that the model was able to reproduce most of the three-dimensional features in the experimental flames. Hence, we feel the model has captured the essential physics in this flame-spreading problem.

However, quantitative comparisons between experiment and model indicate that the presently computed results predict longer flame and pyrolysis lengths, a smaller downstream flame standoff distance, and a wider flammable domain. As was seen in related work on forced flow cases, these differences can be improved by further refining the model, including gas-phase radiation mechanisms, and a better selection (determination) of the kinetic rate constants used in the computation. Despite these differences the model captures the essential physics of upward flame spread phenomena in partial gravity and reduced pressures.

Acknowledgements

This work was supported by the NASA Headquarters Office of Biological and Physical Sciences the Microgravity Science Division, and the NASA Graduate Student Research Program, for which the authors are grateful. We also thank P. Ferkul, R. Pettegrew, and J. Easton for their help with partial gravity experiments aboard the aircraft.